Laser-induced alignment of nanoparticles and macromolecules for single-particle-imaging applications

Muhamed Amin,[1,2,3] Jean-Michel Hartmann,[4] Amit K. Samanta,[1,5] and Jochen Küpper[1,5,6,*]

[1] *Center for Free-Electron Laser Science CFEL, Deutsches Elektronen-Synchrotron DESY, Notkestr. 85, 22607 Hamburg, Germany*
[2] *Rijksuniversiteit Groningen Biomolecular Sciences and Biotechnology Institute, University of Groningen, Groningen, Netherlands*
[3] *Department of Sciences, University College Groningen, University of Groningen, Groningen, Netherlands*
[4] *Laboratoire de Météorologie Dynamique/IPSL, CNRS, Ecole polytechnique, Institut Polytechnique de Paris, Sorbonne Université, Ecole Normale Supérieure, Université PSL, F-91120 Palaiseau, France*
[5] *Center for Ultrafast Imaging, Universität Hamburg, Luruper Chaussee 149, 22761 Hamburg, Germany*
[6] *Department of Physics, Universität Hamburg, Luruper Chaussee 149, 22761 Hamburg, Germany*

(Dated: 2023-06-12)

Laser-induced alignment of particles and molecules was long envisioned to support three-dimensional structure determination using single-particle imaging with x-ray free-electron lasers [PRL 92, 198102 (2004)]. However, geometric alignment of isolated macromolecules has not yet been demonstrated. Using molecular modeling, we analyzed and demonstrated how the alignment of large nanorods and proteins is possible with standard laser technology, and performed a comprehensive analysis on the dependence of the degree of alignment on molecular properties and experimental details. Calculations of the polarizability anisotropy of about 150,000 proteins yielded a skew-normal distribution with a location of 1.2, which reveals that most of these proteins can be aligned using appropriate, realistic experimental parameters. Moreover, we explored the dependence of the degree of alignment on experimental parameters such as particle temperature and laser-pulse energy.

INTRODUCTION

X-ray free-electron lasers (XFELs) promise the diffractive imaging of single molecules and nanoparticles at atomic resolution [1]. Ultra-short, high intensity x-ray pulses interact with individual molecules and using the "diffraction-before-destruction" approach [2, 3] large series of diffraction patterns are collected. Two-dimensional diffraction patterns from randomly oriented samples would then be computationally assembled to a diffraction volume to retrieve the three-dimensional structure [4–6].

In the standard single-particle imaging (SPI) method, the camera images do not contain *a priori* information of the molecules' orientation and, so far, the uncertainty is attacked *in silico* [6]. Significant efforts were made in improving the reconstruction process and the achievable resolution, but it is still a highly challenging task, especially for weakly scattering particles like individual proteins, where diffraction signals from single molecules are generally not strong enough to allow for the averaging and sorting approaches [7, 8]. This is one of the major bottlenecks for atomic-spatial-resolution SPI.

Imaging samples with controlled alignment or orientation [9] allows to significantly mitigate this problem by allowing to sum the diffraction signals from many identically aligned molecules to provide a much stronger signal, thus improving the image reconstruction step and paving the way toward atomic-resolution SPI [3, 10, 11]. Careful analysis of simulated diffraction patterns of laser-aligned proteins demonstrated that it is possible to observe the secondary structure of proteins with only reasonably-strong degrees of alignment $\langle\cos^2\theta\rangle \geq 0.9$ [12].

The alignment of small molecules using external electric fields from moderately intense, nonresonant light pulses was studied extensively using experimental and theoretical methods [13–17]. Strong alignment was achieved for linear, symmetric top, and asymmetric top molecules in the adiabatic [14], intermediate [16, 18], and impulsive regimes [13, 19]. Considerable efforts were made for laser-induced alignment of large molecules [20–22] and even for some complex and floppy polyatomic molecules [23] as well as for weakly bound molecular complexes [24]. Such aligned-molecule samples were also studied by electron [25, 26] and x-ray diffractive imaging experiments [27]. Possibilities to laser-align large biomolecules without deterioration of the secondary structure were proposed [3, 10], but, so far, no alignment for such systems has been reported.

For macromolecules, there are several challenges for achieving the required alignment. Theoretical predictions supported by *in silico* analysis can be a very important step to guide the experiments. However, atomistic molecular dynamics (MD) simulations are computationally very expensive for large particles, especially when the interaction time extends to hundreds of nanoseconds [28]. In addition, to accurately predict the "ensemble averaged" single-particle diffraction images of macromolecules, simulation of a large distribution of particles is essential rather than a single particle. Ensemble computations are also crucial for studying the temperature effects, as this can be an important factor in preserving the secondary structures of macromolecules, like proteins, and this step makes MD simulations even more computationally expensive.

In this work, we predicted and analyzed the laser-induced alignment of (bio-)nanoparticles. Nanoparticles and proteins were treated as rigid bodies, supported by previous molecular-dynamics simulations of structural changes in strong electric fields [29]. The key parameters for such simulations are the overall polarizability, shape and their anisotropy, the temperature of the macromolecules, and the alignment laser field. We disentangled how these parameters can be tuned for maximum alignment of gold-nanorod model systems and how this can be exploited for the strong laser alignment of biological macromolecules, e. g., proteins.

COMPUTATIONAL METHODS

The response of the particles to a nonresonant external electric field was calculated based on their polarizability tensors, which yielded the time-dependent induced dipole moments. For metallic nanorods, the polarizabilities were directly obtained by solving Laplace's equation with Dirichlet boundary conditions and using Monte Carlo path integral methods [30]. For proteins, the polarizabilities were derived from the same calculations using regression-based scaling [31, 32].

Molecular ensembles were set up with random initial phase-space distributions, i. e., with initial angular velocities according to a Boltzmann distribution at the given temperature and with random initial angular positions. Each run included 20,000 particles. The angular positions of particles were stored in quaternions throughout the calculation. The inertial tensors of the artificial nanorods were calculated for cylinders. However, for proteins the tensors were calculated based on the atomic masses and coordinates as available from the protein data bank (PDB) [33].

Electric fields of the alignment-laser pulses were represented by Gaussian functions with variable peak intensities. For simplicity, we used a temporal full-width at half maximum (FWHM) of 8 ns, corresponding to the typical pulse duration of standard Q-switched Nd:YAG lasers, often used in alignment experiments. We also assumed typical linearly polarized laser pulses with intensities of $10^{10} \ldots 10^{12}$ W/cm^2.

The particles' angular phase-space positions were propagated in time by integrating Euler's equations of angular motion using a new, Python-based, openly available software package CMIclassirot [34], which was based on and checked against previous classical-alignment computations [35]. All simulations propagated the particles for 50 ns, except for the alignment of gold nanoparticles in Fig. 1, for which the simulation time was extended to 200 ns. The effect of resonances was ignored in the simulation, i. e., the laser-field frequency was assumed to be far off resonance from the molecules and nanoparticles absorption.

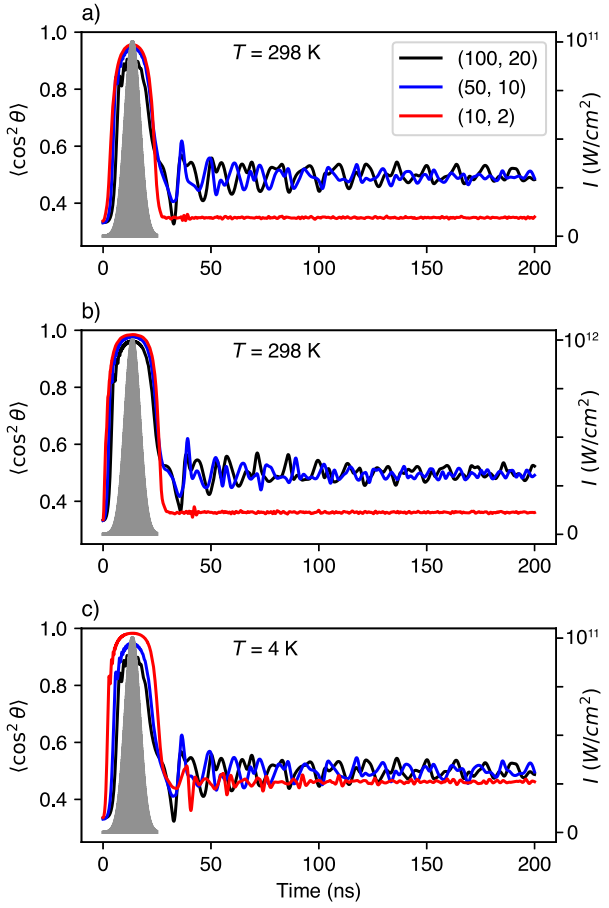

FIG. 1. Degree of alignment of gold nanorods for different temperatures (T) and laser-field intensities (I). a) $T = 298$ K and $I = 10^{11}$ W/cm^2. b) $T = 298$ K and $I = 10^{12}$ W/cm^2. and c) $T = 4$ K and $I = 10^{11}$ W/cm^2. The degree of alignment of (10, 2) rods is shown in red, (50, 10) in blue, and (100, 20) in black. The temporal laser profile is indicated by the shaded gray area and the corresponding field intensities are specified on the secondary axes. Please see the text for details and definitions of the abbreviations.

RESULTS

The computed time-dependent degrees of laser-induced alignment of nanorods of three different sizes are shown in Fig. 1 for 298 K and 4 K and alignment-laser peak intensities of $10^{11} \ldots 10^{12}$ W/cm^2. Throughout this manuscript, nanorod sizes are represented as ($height$/nm, $diameter$/nm), with the calculations performed for (10, 2), (50, 10), (100, 20), respectively.

During the pulse and with particles initially at room temperature, the degree of alignment for all three particles' sizes, Fig.1 a, b, follows the temporal laser profile on the rising edge in a quasi-adiabatic fashion [16]. The smallest particle (10, 2) exhibits the largest alignment of $\langle \cos^2\theta \rangle = 0.96$.

However, the laser turn-off dynamics show considerable differences: The two larger nanorods exhibit permanent alignment after the laser pulse is turned off, whereas the small nanorod quasi-adiabatically follows the temporal laser profile to an isotropic field-free angular distribution, i. e., $\langle\cos^2\theta\rangle = 1/3$. This can be rationalized by comparing the rotation periods of the nanorods, i. e., the average time needed for each nanorod to rotate around its center of mass by 360 °, to the alignment-laser-pulse duration. The rotation periods depend on the temperature, because the initial phase space is assigned based on a corresponding Boltzmann distribution. For large nanorods at room temperature, the rotational periods are within 10 µs ($\nu \approx 100$ kHz, $\omega \approx 6.3 \cdot 10^5$ rad/s), which is three orders of magnitude larger than the pulse duration. Thus, these particles exhibit non-adiabatic alignment, resulting in a permanent alignment after the pulse is off, Fig. 1 a, b. Already at low intensity, $I = 10^{11}$ W/cm^2, the particles are confined even after the laser is off to fully rotate in a plane containing the laser polarization vector, corresponding to $\langle\cos^2\theta\rangle = 0.5$, Fig. 1 a. Thus, no increase in the permanent alignment is possible at $I = 10^{12}$ W/cm^2, Fig. 1 b. For small nanorod, the rotational period reduces to 20 ns, which is comparable to the alignment-laser pulse duration. Thus, these particles exhibit quasi-adiabatic alignment [16, 18] and no permanent alignment is observed after the pulse, Fig. 1 a, b.

However, at 4 K, which is experimentally achievable [36], the rotational period increases to 400 ns for the (10, 2) rods, resulting in the transition to the non-adiabatic regime and thus a field-free permanent alignment is observed even for this smallest rod after the pulse is off, see Fig. 1 c.

For the larger nanorods (blue, black) the degree of permanent alignment after the pulse shows a strong oscillation that decays with time, which is a result of the slow dephasing between the rotations of the confined nanorods, which start to rotate with different angular velocities, but significantly slower than for the small particles. This variation in the angular velocities causes the decay of the pattern with time. Furthermore, to ensure that these oscillations were not a result of undersampling, we performed a convergence study in which we increased the number of particles for the large nanorods to 200,000 particles and we obtained the same oscillations.

Although all our simulations take into account the full polarizability tensor, it is instructive to study the degree of alignment as a function of the nanorod shape described by the ratio of its principal moments of polarizability, i. e., the ratio of $\alpha_\parallel$ to $\alpha_\perp$, which correlates with the polarizability anisotropy:

$$\begin{aligned} \alpha_\parallel &= \max\left(\alpha_{11}, \alpha_{22}, \alpha_{33}\right) \\ \alpha_\perp &= \left(3\alpha - \alpha_\parallel\right)/2 \\ \alpha_r &= \alpha_\parallel/\alpha_\perp \end{aligned} \tag{1}$$

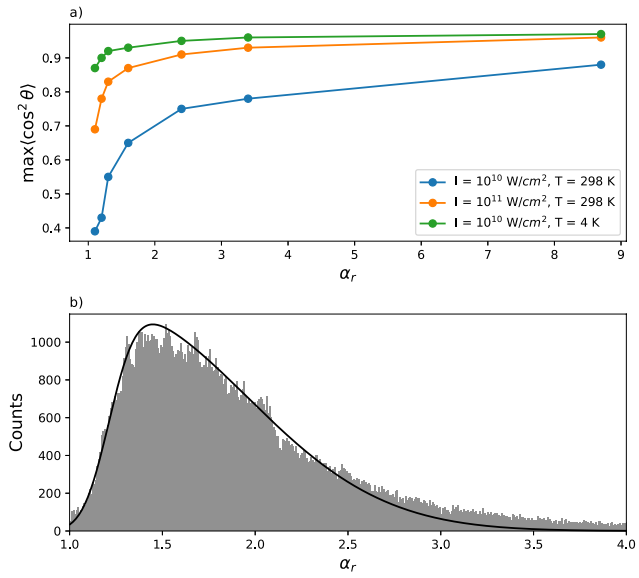

FIG. 2. a) Maximum degree of alignment, $\max\langle\cos^2\theta\rangle$, as a function of the polarizability ratio α_r at different temperatures and intensities for a nonorod of 10π nm^3. At low temperature a high degree of alignment is achieved even at very low intensity. b) The α_r distribution of about 150,000 proteins in the protein data bank (PDB) approximately follows a skew-normal distribution with a location of 1.2, scale of 0.7 and skewness parameter of 6.5.

with the static-polarizability components in the principal axes of polarizability frame α_{ii} and $\alpha = \sum \alpha_{ii}$. For α_r the scaling factor applied to the elements of the polarizability tensors to account for the dielectric medium of proteins cancels out, and does not have to be included in this discussion of shape.

Fig. 2 a shows the dependence of the maximum degree of alignment i. e., $\max\langle\cos^2\theta\rangle$ on α_r for two different laser peak intensities of $I = 10^{10}$ W/cm^2 and $I = 10^{11}$ W/cm^2. There is a quick rise of $\max\langle\cos^2\theta\rangle$ for α_r in the range $1.2 \ldots 2.5 \cdot 10^{10}$ W/cm^2, depending on temperature, confirming that with increasing particle anisotropy there is a significant increase in the maximum degree of alignment, as could be expected. Further increasing α_r led to a further slow increase in the maximum alignment toward an asymptotic maximum. Furthermore, for higher intensity one observes stronger alignment, especially for small values of α_r. The same holds for lower temperatures, which enable significantly increased alignment even at lower laser intensities [20, 37]. Specifically, for 10^{10} W/cm^2 and room-temperature particles it requires $\alpha_r > 8$ to obtain a reasonable degree of alignment of $\langle\cos^2\theta\rangle > 0.8$, whereas at low temperature (4 K) [36], strong alignment of $\langle\cos^2\theta\rangle = 0.9$ is achieved even at $\alpha_r = 1.5$.

Proteins and similar biological macromolecules are the principal target for single particle imaging. Thus, we calculated the polarizability ratio α_r of about 150,000

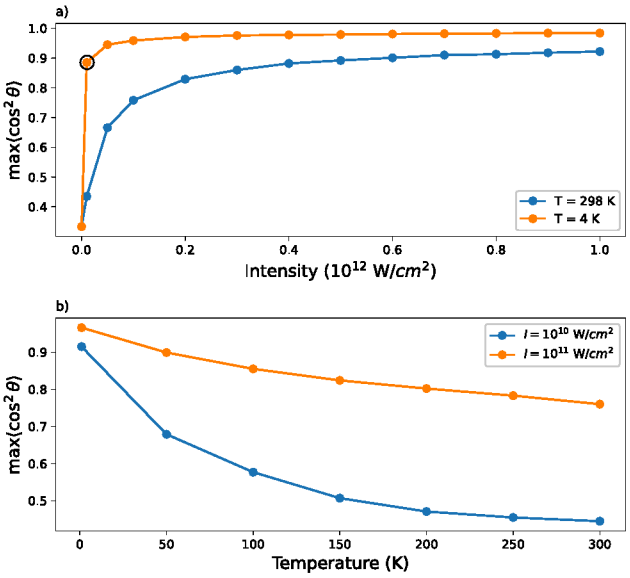

FIG. 3. a) The effect of laser pulse intensity on the degree of alignment of a gold nanorod with $\alpha_r = 1.2$ and size (3.6, 3.2) at 298 K (blue) and 4 K (orange). A good degree of alignment $\max\left\langle\cos^2\theta\right\rangle = 0.9$ is achieved at 4 K with intensities as low as of 10^{10} W/cm^2 (filled circles). However, a significantly stronger intensities (more than $5 \cdot 10^{11}$ W/cm^2) are required to obtain a good degree of alignment at 298 K. b) The effect of temperature on the degree of alignment of the same gold nanorod (polarizability ratio of 1.2) for two different laser intensities, 10^{10} W/cm^2 (blue) and 10^{11} W/cm^2 (orange). Strong alignment is achieved for both intensities at very low temperatures. However, a quick decay in the $\max\left\langle\cos^2\theta\right\rangle$ is observed for the low intensity with increasing the temperature.

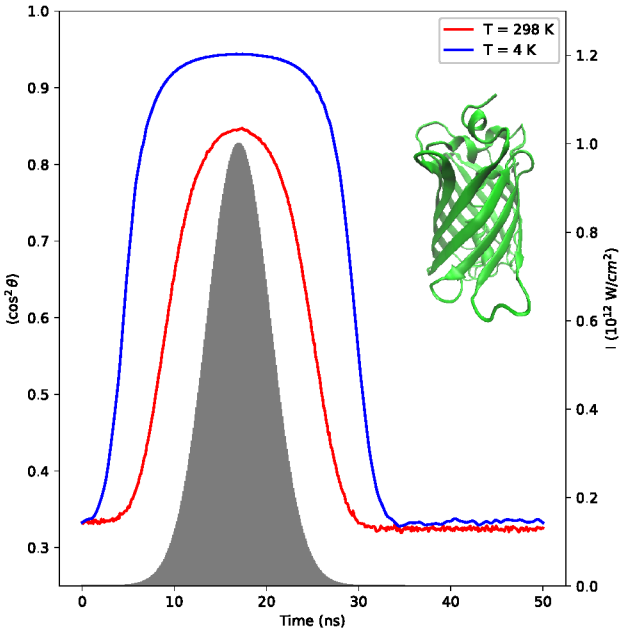

FIG. 4. Degree of alignment of the green fluorescent protein, depicted in the inset, at 298 K (red) and 4 K (blue) using 10^{12} W/cm^2 pulse intensity (shaded area in gray). In consistency with Fig. 3, a good degree of alignment of $\left\langle\cos^2\theta\right\rangle = 0.84$ is achieved at 4 K even at very low intensities, e. g., in the raising flank of the laser pulse at $5 \cdot 10^{10}$ W/cm^2. However, a stronger intensity of 10^{12} W/cm^2 is required to achieve similar alignment at room temperature.

proteins using the database we built previously [32], see Fig. 2 b. These data were obtained by calculating the polarizability tensors of proteins based on their PDB structures using ZENO [30, 32]. These tensors were diagonalized to put all molecules in the polarizability frame, their α_r values were computed according to (1), and summarized in the histogram in Fig. 2 b. The α_r distribution follows a skew-normal distribution with a location of ∼1.2. As 96 % of the data have an α_r larger than the location value, this distribution directly indicates that a corresponding, significant fraction of these proteins have sufficiently anisotropic polarizabilities that make them directly amenable to strong laser alignment.

To provide further understanding of the effect of shape of the object on the maximum achieved alignment, we studied the effect of laser intensity and particle temperature for a gold nanorod with $\alpha_r = 1.2$ and size (3.6, 3.2), see Fig. 3.

Fig. 3 a shows the effect of different laser intensities on the degree of alignment at 298 K and 4 K. The degree of alignment quickly increases at low intensities, depending on temperature, and saturates toward the asymptotic limit (*vide supra*). Again, the achievable degree of alignment at 4 K is significantly higher than at room temperature. In the latter case, strong alignment of $\max\left\langle\cos^2\theta\right\rangle = 0.9$ is achieved for the highest intensities of 10^{12} W/cm^2, whereas a 4 K sample enables very strong alignment of $\max\left\langle\cos^2\theta\right\rangle = 0.95$ for intensities as low as $5 \cdot 10^{10}$ W/cm^2.

Similarly, Fig. 3 b shows the degree of alignment for the same particle versus the temperature at two different laser intensities, demonstrating the decrease of alignment with increasing temperature, especially so for weaker laser intensities.

Thus, based on our model system, which is a nanorod with an anisotropy similar to that of most of the proteins, Fig. 2, a good degree of alignment is achievable for most proteins at 298 K using 10 ns alignment-laser pulses with peak intensities around 10^{11} W/cm^2. This alignment can be improved significantly exploiting cryogenically cooled (4 K) [36] proteins even with a much weaker laser pulse. Furthermore, the cooling will also reduce the chance of structural damage of proteins by intense laser fields [29].

To simulate the alignment of an actual protein, we have applied our method to simulate laser-induced alignment of the prototypical green fluorescent protein (GFP), which has a cylindrical shape ($\alpha_r = 1.5$) and thus strong

alignment could be expected, see Fig. 2. We calculated the inertia and polarizability tensors based on the PDB structure with PDBID 1GFL [38]. The elements of the polarizability tensors were scaled by a factor of 0.4 to account for the dielectric medium of proteins ($\epsilon_r = 3.2$ [32]). Then, we applied a Gaussian laser pulse with a FWHM of 8 ns. As shown in Fig. 4, moderate alignment of $\max\left\langle\cos^2\theta\right\rangle = 0.84$ was obtained at room temperature for a peak intensity of 10^{12} W/cm^2. However, at 4 K $\max\left\langle\cos^2\theta\right\rangle = 0.85$ was already achieved for $2 \cdot 10^{10}$ W/cm^2 and for 10^{12} W/cm^2 we obtained $\max\left\langle\cos^2\theta\right\rangle = 0.94$.

In summary, using simulations based on the classical dynamics of rigid bodies we showed that significant laser-induced alignment of nanorods and biological macromolecules, with typical polarizability ratios $\alpha_\parallel/\alpha_\perp$, can be achieved. The dependence of the degree of alignment on the alignment-laser intensity, sample temperature, and molecular size and polarizability were analyzed. We showed that a very high degree of alignment can be achieved for cryogenically-cooled [36] proteins at a moderate laser power of 10^{10} W/cm^2, which should not cause radiation damage [29]. This high degree of control of $\left\langle\cos^2\theta\right\rangle \geq 0.94$ paves the way for future atomic resolution [12] single particle x-ray and electron diffractive imaging experiments. Furthermore, the achievable atomic spatial and femtosecond temporal resolution provide the prerequisites for future time resolved studies of ultrafast biochemical dynamics.

Our approach provides clear insight into the optical control of macromolecules and enables better modeling of the experimental parameters for successful laser-induced alignment experiments, which are currently in progress in our group. Envisioned future experiments plan to make use of our cryogenic nanoparticle cooling setup [36] together with efficient laser control to achieve a very high degree of alignment for shock-frozen proteins and, in turn, sub-nanometer resolution in single particle x-ray imaging. We believe that this framework will prove useful for furthering the field of single-particle x-ray imaging and would allow us to observe atomically resolved snapshots of ultrafast chemical dynamics.

The achievable strong laser alignment of nanoscopic objects could have further applications in nanoscience [39] as well as in nanoscale quantum optics or quantum sensing [40].

ACKNOWLEDGMENT

We acknowledge financial support by Deutsches Elektronen-Synchrotron DESY, a member of the Helmholtz Association (HGF) and the use of the Maxwell computational resources operated at DESY. This work has been supported by the European Research Council under the European Union's Seventh Framework Program (FP7/2007-2013) through the Consolidator Grant COMOTION (614507) and the Cluster of Excellence "Advanced Imaging of Matter" (AIM, EXC 2056, ID 390715994) of the Deutsche Forschungsgemeinschaft (DFG).

CODE AVAILABILITY

Classical rotational dynamics simulations were performed using CMIclassrot, available at `https://github.com/CFEL-CMI/CMIclassirot.git`.

* Email: jochen.kuepper@cfel.de; website: https://www.controlled-molecule-imaging.org

[1] R. Neutze, R. Wouts, D. van der Spoel, E. Weckert, and J. Hajdu, Potential for biomolecular imaging with femtosecond x-ray pulses, Nature **406**, 752 (2000).

[2] M. J. Bogan, W. H. Benner, S. Boutet, U. Rohner, M. Frank, A. Barty, M. M. Seibert, F. Maia, S. Marchesini, S. Bajt, B. Woods, V. Riot, S. P. Hau-Riege, M. Svenda, E. Marklund, E. Spiller, J. Hajdu, and H. N. Chapman, Single particle x-ray diffractive imaging, Nano Lett. **8**, 310 (2008).

[3] A. Barty, J. Küpper, and H. N. Chapman, Molecular imaging using x-ray free-electron lasers, Annu. Rev. Phys. Chem. **64**, 415 (2013).

[4] H. N. Chapman, X-ray imaging beyond the limits, Nature Mater. **8**, 299 (2009).

[5] M. M. Seibert, T. Ekeberg, F. R. N. C. Maia, M. Svenda, J. Andreasson, O. Jönsson, D. Odić, B. Iwan, A. Rocker, D. Westphal, M. Hantke, D. P. Deponte, A. Barty, J. Schulz, L. Gumprecht, N. Coppola, A. Aquila, M. Liang, T. A. White, A. Martin, C. Caleman, S. Stern, C. Abergel, V. Seltzer, J.-M. Claverie, C. Bostedt, J. D. Bozek, S. Boutet, A. A. Miahnahri, M. Messerschmidt, J. Krzywinski, G. Williams, K. O. Hodgson, M. J. Bogan, C. Y. Hampton, R. G. Sierra, D. Starodub, I. Andersson, S. Bajt, M. Barthelmess, J. C. H. Spence, P. Fromme, U. Weierstall, R. Kirian, M. Hunter, R. B. Doak, S. Marchesini, S. P. Hau-Riege, M. Frank, R. L. Shoeman, L. Lomb, S. W. Epp, R. Hartmann, D. Rolles, A. Rudenko, C. Schmidt, L. Foucar, N. Kimmel, P. Holl, B. Rudek, B. Erk, A. Hömke, C. Reich, D. Pietschner, G. Weidenspointner, L. Strüder, G. Hauser, H. Gorke, J. Ullrich, I. Schlichting, S. Herrmann, G. Schaller, F. Schopper, H. Soltau, K.-U. Kühnel, R. Andritschke, C.-D. Schröter, F. Krasniqi, M. Bott, S. Schorb, D. Rupp, M. Adolph, T. Gorkhover, H. Hirsemann, G. Potdevin, H. Graafsma, B. Nilsson, H. N. Chapman, and J. Hajdu, Single mimivirus particles intercepted and imaged with an X-ray laser, Nature **470**, 78 (2011).

[6] K. Ayyer, P. L. Xavier, J. Bielecki, Z. Shen, B. J. Daurer, A. K. Samanta, S. Awel, R. Bean, A. Barty, M. Bergemann, T. Ekeberg, A. D. Estillore, H. Fangohr, K. Giewekemeyer, M. S. Hunter, M. Karnevskiy, R. A. Kirian, H. Kirkwood, Y. Kim, J. Koliyadu, H. Lange, R. Letrun, J. Lübke, T. Michelat, A. J. Morgan, N. Roth, T. Sato, M. Sikorski, F. Schulz, J. C. H. Spence, P. Vagovic, T. Wollweber, L. Worbs, O. Yefanov,

Y. Zhuang, F. R. N. C. Maia, D. A. Horke, J. Küpper, N. D. Loh, A. P. Mancuso, and H. N. Chapman, 3D diffractive imaging of nanoparticle ensembles using an x-ray laser, Optica **8**, 15 (2021), arXiv:2007.13597 [physics].

[7] K. Ayyer, O. M. Yefanov, D. Oberthür, S. Roy-Chowdhury, L. Galli, V. Mariani, S. Basu, J. Coe, C. E. Conrad, R. Fromme, A. Schaffer, K. Dörner, D. James, C. Kupitz, M. Metz, G. Nelson, P. L. Xavier, K. R. Beyerlein, M. Schmidt, I. Sarrou, J. C. H. Spence, U. Weierstall, T. A. White, J.-H. Yang, Y. Zhao, M. Liang, A. Aquila, M. S. Hunter, J. S. Robinson, J. E. Koglin, S. Boutet, P. Fromme, A. Barty, and H. N. Chapman, Macromolecular diffractive imaging using imperfect crystals, Nature **530**, 202 (2016).

[8] K. Ayyer, Reference-enhanced x-ray single-particle imaging, Optica **7**, 593 (2020), arXiv:2002.10267 [physics].

[9] We distiguish molecular alignment and orientation according to the usual convention [15], i. e., alignment refers to fixing the molecules along certain axes whereas orientation refers to the breaking of the "up-down" (mirror) symmetry along these axes.

[10] J. C. H. Spence and R. B. Doak, Single molecule diffraction, Phys. Rev. Lett. **92**, 198102 (2004).

[11] F. Filsinger, G. Meijer, H. Stapelfeldt, H. Chapman, and J. Küpper, State- and conformer-selected beams of aligned and oriented molecules for ultrafast diffraction studies, Phys. Chem. Chem. Phys. **13**, 2076 (2011), arXiv:1009.0871 [physics].

[12] J. C. H. Spence, K. Schmidt, J. S. Wu, G. Hembree, U. Weierstall, R. B. Doak, and P. Fromme, Diffraction and imaging from a beam of laser-aligned proteins: resolution limits, Acta Cryst. A **61**, 237 (2005).

[13] F. Rosca-Pruna and M. J. J. Vrakking, Experimental observation of revival structures in picosecond laser-induced alignment of I_2, Phys. Rev. Lett. **87**, 153902 (2001).

[14] J. J. Larsen, H. Sakai, C. P. Safvan, I. Wendt-Larsen, and H. Stapelfeldt, Aligning molecules with intense nonresonant laser fields, J. Chem. Phys. **111**, 7774 (1999).

[15] H. Stapelfeldt and T. Seideman, Colloquium: Aligning molecules with strong laser pulses, Rev. Mod. Phys. **75**, 543 (2003).

[16] S. Trippel, T. Mullins, N. L. M. Müller, J. S. Kienitz, J. J. Omiste, H. Stapelfeldt, R. González-Férez, and J. Küpper, Strongly driven quantum pendulum of the carbonyl sulfide molecule, Phys. Rev. A **89**, 051401(R) (2014), arXiv:1401.6897 [quant-ph].

[17] C. P. Koch, M. Lemeshko, and D. Sugny, Quantum control of molecular rotation, Rev. Mod. Phys. **91**, 035005 (2019).

[18] S. Trippel, T. G. Mullins, N. L. M. Müller, J. S. Kienitz, K. Długołęcki, and J. Küpper, Strongly aligned and oriented molecular samples at a kHz repetition rate, Mol. Phys. **111**, 1738 (2013), arXiv:1301.1826 [physics].

[19] E. T. Karamatskos, S. Raabe, T. Mullins, A. Trabattoni, P. Stammer, G. Goldsztejn, R. R. Johansen, K. Długołęcki, H. Stapelfeldt, M. J. J. Vrakking, S. Trippel, A. Rouzée, and J. Küpper, Molecular movie of ultrafast coherent rotational dynamics of OCS, Nat. Commun. **10**, 3364 (2019), arXiv:1807.01034 [physics].

[20] L. Holmegaard, J. H. Nielsen, I. Nevo, H. Stapelfeldt, F. Filsinger, J. Küpper, and G. Meijer, Laser-induced alignment and orientation of quantum-state-selected large molecules, Phys. Rev. Lett. **102**, 023001 (2009), arXiv:0810.2307 [physics].

[21] T. Mullins, E. T. Karamatskos, J. Wiese, J. Onvlee, A. Rouzée, A. Yachmenev, S. Trippel, and J. Küpper, Picosecond pulse-shaping for strong three-dimensional field-free alignment of generic asymmetric-top molecules, Nat. Commun. **13**, 1431 (2022), arXiv:2009.08157 [physics].

[22] D. Pentlehner, J. H. Nielsen, L. Christiansen, A. Slenczka, and H. Stapelfeldt, Laser-induced adiabatic alignment of molecules dissolved in helium nanodroplets, Phys. Rev. A **87**, 063401 (2013).

[23] A. S. Chatterley, C. Schouder, L. Christiansen, B. Shepperson, M. H. Rasmussen, and H. Stapelfeldt, Long-lasting field-free alignment of large molecules inside helium nanodroplets, Nat. Commun. **10**, 133 (2019).

[24] S. Trippel, J. Wiese, T. Mullins, and J. Küpper, Communication: Strong laser alignment of solvent-solute aggregates in the gas-phase, J. Chem. Phys. **148**, 101103 (2018), arXiv:1801.08789 [physics].

[25] S. T. Park, A. Gahlmann, Y. He, J. S. Feenstra, and A. H. Zewail, Ultrafast electron diffraction reveals dark structures of the biological chromophore indole, Angew. Chem. Int. Ed. **47**, 9496 (2008).

[26] C. J. Hensley, J. Yang, and M. Centurion, Imaging of isolated molecules with ultrafast electron pulses, Phys. Rev. Lett. **109**, 133202 (2012).

[27] J. Küpper, S. Stern, L. Holmegaard, F. Filsinger, A. Rouzée, A. Rudenko, P. Johnsson, A. V. Martin, M. Adolph, A. Aquila, S. Bajt, A. Barty, C. Bostedt, J. Bozek, C. Caleman, R. Coffee, N. Coppola, T. Delmas, S. Epp, B. Erk, L. Foucar, T. Gorkhover, L. Gumprecht, A. Hartmann, R. Hartmann, G. Hauser, P. Holl, A. Hömke, N. Kimmel, F. Krasniqi, K.-U. Kühnel, J. Maurer, M. Messerschmidt, R. Moshammer, C. Reich, B. Rudek, R. Santra, I. Schlichting, C. Schmidt, S. Schorb, J. Schulz, H. Soltau, J. C. H. Spence, D. Starodub, L. Strüder, J. Thøgersen, M. J. J. Vrakking, G. Weidenspointner, T. A. White, C. Wunderer, G. Meijer, J. Ullrich, H. Stapelfeldt, D. Rolles, and H. N. Chapman, X-ray diffraction from isolated and strongly aligned gas-phase molecules with a free-electron laser, Phys. Rev. Lett. **112**, 083002 (2014), arXiv:1307.4577 [physics].

[28] F. Noé, Beating the millisecond barrier in molecular dynamics simulations, Biophys. J. **108**, 228 (2015).

[29] E. G. Marklund, T. Ekeberg, M. Moog, J. L. P. Benesch, and C. Caleman, Controlling protein orientation in vacuum using electric fields, J. Phys. Chem. Lett. **8**, 4540–4544 (2017).

[30] D. Juba, D. J. Audus, M. Mascagni, J. F. Douglas, and W. Keyrouz, ZENO: Software for calculating hydrodynamic, electrical, and shape properties of polymer and particle suspensions, J. Res. Nat. Inst. Stand. Tech. **122**, 20 (2017).

[31] M. Amin, H. Samy, and J. Küpper, Robust and accurate computational estimation of the polarizability tensors of macromolecules, J. Phys. Chem. Lett. **10**, 2938 (2019), arXiv:1904.02504 [physics].

[32] M. Amin and J. Küpper, Variations in proteins dielectric constants, ChemistryOpen **9**, 691–69 (2020).

[33] H. M. Berman, J. Westbrook, Z. Feng, G. Gilliland, T. N. Bhat, H. Weissig, I. N. Shindyalov, and P. E. Bourne, The Protein Data Bank, Nucleic Acids Research **28**, 235 (2000).

[34] M. Amin and J. Küpper, CMIclassirot: Classical-physics simulations of laser alignment, `https://github.com/CFEL-CMI/CMIclassirot.git`, Software package (2023).

[35] J. M. Hartmann and C. Boulet, Quantum and classical approaches for rotational relaxation and nonresonant laser alignment of linear molecules: A comparison for co2 gas in the nonadiabatic regime, J. Chem. Phys. **136**, 184302 (2012).

[36] A. K. Samanta, M. Amin, A. D. Estillore, N. Roth, L. Worbs, D. A. Horke, and J. Küpper, Controlled beams of shockfrozen, isolated, biological and artificial nanoparticles, Struct. Dyn. **7**, 024304 (2020), arXiv:1910.12606 [physics].

[37] V. Kumarappan, C. Z. Bisgaard, S. S. Viftrup, L. Holmegaard, and H. Stapelfeldt, Role of rotational temperature in adiabatic molecular alignment, J. Chem. Phys. **125**, 194309 (2006).

[38] F. Yang, L. Moss, and G. Phillips Jr., The molecular structure of green fluorescent protein, Nat. Biotechnol. **14**, 1246 (1996).

[39] M. Krajewski, Magnetic-field-induced synthesis of magnetic wire-like micro- and nanostructures, Nanoscale **9**, 16511 (2017).

[40] B. A. Stickler, K. Hornberger, and M. S. Kim, Quantum rotations of nanoparticles, Nat. Rev. Phys. **3**, 589 (2021), 2102.00992.